Coupling between Structural Deformation and Attitude Motion of Large Planar Space Structures Suspended by Multi-Tethers

By Kosei ISHIMURA[1)] and Ken HIGUCHI[2)]

[1)] *Graduate School of Information Science and Technology, Hokkaido University, N14-W9,Sapporo, Japan,060-0814*
[2)] *Institute of Space and Astronautical Science/Japan Aerospace Exploration Agency, (ISAS/JAXA), 3-1-1 Yoshinodai,Sagamihara, Japan,229-8510*

A planar space structure suspended by multi-tethers is one candidate for large and lightweight structures. For such flexible structures, coupling phenomena between structural deformation and attitude motion must be considered. In the present paper, the dynamic characteristics of a planar structure suspended by multi-tethers are investigated. Simulation results reveal that the coupling occurs for low tether stiffness. In addition, it is shown that the coupling can also occur if a number of the tethers become slack. Thermal deformation of the planar structure is one cause of tether slack. Thermal deformation and the induced attitude motion are also investigated. It is shown that roll and yaw motions become unstable due to thermal deformation. Finally, we modify the condition of the connection between sub-panels in order to reduce the overall thermal deformation, and it is confirmed that large deformation can be inhibited by the modification.

Key Words: Structural Analysis, Spacecraft Dynamics, Attitude Motion

Nomenclature

A_t : cross section of a tether

C_{OB_pq} : element (p,q) of the direction cosine matrix between the body and orbital coordinates

$\mathbf{C}_l, \mathbf{C}_{rx}, \mathbf{C}_{ry}, \mathbf{C}_{rxx}\mathbf{C}_{ryy}$: coefficient matrixes due to the mass distribution of the panel

$\mathbf{C}_m, \mathbf{C}_p, \mathbf{C}_t$: damping matrixes due to kinetic energy, strain energy of the panel, and strain energy of the tethers, respectively

E_t : Young's modulus of the tethers

$\mathbf{f}_g, \mathbf{f}_m, \mathbf{f}_T$: force vectors due to gravitational potential energy, kinetic energy, and thermal stress, respectively.

I_x, I_y, I_z : moments of inertia of the panel

k_T : coefficient of thermal stress

$\mathbf{K}_e, \mathbf{K}_g, \mathbf{K}_m, \mathbf{K}_p, \mathbf{K}_t$: stiffness matrixes of a finite element, due to gravitational potential energy, kinetic energy, strain energy of the panel, and strain energy of the tethers, respectively

l_{ij} : natural length of the tether at node (i,j)

l_v : vertical component of natural length of tethers

M, m_b, m_p, m_r : total mass ($= m_b + m_p$), mass of bus component, mass of the panel, and mass ratio ($= m_p / M$), respectively

$\mathbf{M}, \mathbf{M}_p$: total mass matrix and mass matrix of the panel, respectively

R : orbital radius

w_{ij} : panel displacement along the -z axis at node (i,j)

δ_T : temperature difference between top and bottom sides of the panel

$\boldsymbol{\delta}, \boldsymbol{\delta}_e, \boldsymbol{\delta}_{ij}$: displacement vectors at all nodes, at each element, and at each node (i,j) , respectively

θ , $\dot{\theta}$: true anomaly and orbital angular velocity

$\theta_x, \theta_y, \theta_z$: 3-2-1 Euler angles. In the following, subscripts x, y and z correspond to roll, pitch and yaw axes, respectively

μ : geocentric gravitational constant

ρ : panel mass per unit area

ϕ_x, ϕ_y : rotation of finite element of the panel

$\omega_x, \omega_y, \omega_z$: angular velocities

1. Introduction

Increased size is one of the tendencies of recent space structures such as space antennas, space telescopes, the International Space Station (ISS) and the Space Solar Power

System (SSPS). In the present paper, we focus on large planar structures that have a wide area. Due to lightweight requirements, these large planar structures tend to be flexible. A planar space structure suspended by multi-tethers is a candidate for such large and lightweight structures.

For large and flexible space structures, the deformation of the structure could affect the attitude motion. Although the coupling between structural deformation/vibration and attitude motion for long and narrow structures has been investigated extensively [1-3], research of planar structures is less common [4]. Furthermore, in the planar structures stabilized by tensile forces, tether slack is a significant problem because the dynamic characteristics of such structures could change drastically when the tension of any of the tethers becomes zero. Thermal deformation is one cause of tether slack. Few studies have investigated the effect of thermal deformation on attitude motion for structures other than one-dimensional structures such as long solar-arrays and flexible booms [5-7]. In the present paper, the dynamic characteristics of a planar structure suspended by multi-tethers are investigated. In addition to it, the thermal deformation of the structure and the induced attitude motion are also analyzed.

The investigated structure is a planar structure suspended by multi-tethers, as shown in Fig. 1, the configuration of which is similar to that of the SSPS [8-9] proposed by ISAS/JAXA and USEF. The SSPS is a representative of the structures discussed in the present paper. The SSPS consists of a bus, a panel and multiple tethers. The system utilizes passive gravity-gradient stabilization and has multi-tethers arranged as in a suspension bridge. The entire system consists of small sub-panels that are suspended by tethers at the corners. The SSPS is assumed to be constructed in LEO (500 [km]) and operated in GEO. Due to the similarity, the natural frequency of attitude motion of the analyzed model is almost identical to that of the SSPS.

This paper is organized as follows. In Section 2, we derive Lagrange's equation of motion of the space structure. In the equation, attitude motion, orbital motion and the panel deformation including thermal one are considered. In Section 3, fundamental dynamic characteristics of the structure are shown. At first in the section, natural frequencies and mode shapes at the equilibrium point are calculated to evaluate the coupling between structural deformation and attitude motion. Next, the effect of tether stiffness on the natural frequency is investigated. In Section 4, the effect of tether slack due to thermal deformation is studied. We calculate natural frequencies and mode shapes for the structure with tether slack due to thermal deformation. Furthermore in the section, to demonstrate the coupling between structural deformation and attitude motion, dynamic simulations with periodic thermal input in orbit are carried out. In Section 5, we propose a modified planar structure that can release the thermal deformation locally in order to suppress overall deformation. The effectiveness is shown through numerical simulation. Finally, in Section 6, we offer some concluding remarks.

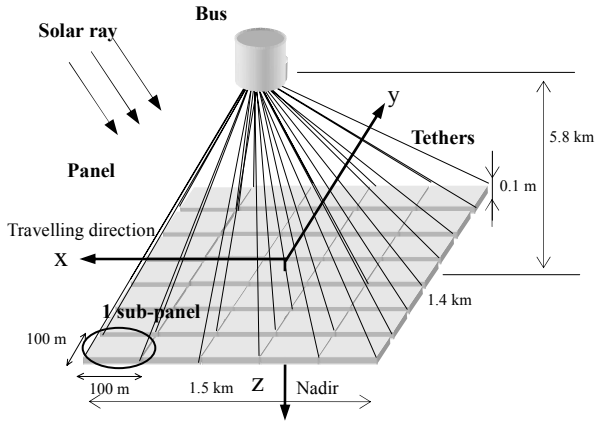

Fig. 1. Analytical model

2. Analytical Model

2.1. Model parameters

The parameters of the analyzed structure are listed in Table 1. The panel is constructed of sandwich panels formed by two thin skins (0.5 [mm]) separated by 0.1 [m]. In the analysis, the bus is modeled as a particle, and the tethers are modeled as mass-less nonlinear springs having spring constants that become zero at compression. The panel is modeled using FEM with 12 DOFs plate-bending elements. Because the natural frequency of in-plane bending is so much higher than that of out-of-plane bending, the panel may be regarded as rigid during in-plane motion. The panel is divided into sub-panels (100×100 [m]), the corners of which are suspended by tethers. The sub-panel is modeled as one finite element with 12 DOFs. The nodes are numbered as shown in Fig. 2. The vertical distance between the bus and the panel is set to 5.8 [km] when the tethers are of natural length. The natural length of each tether is defined as the distance between each sub-panel node and the bus when the panel is flat with no deformation and the tethers bear no load. If the distance between each node and the bus becomes less than the natural length of tether, then the tether is defined to be slack and its spring constant is set to zero.

Table 1 Parameters of the analytical model

bus	mass: m_b	3.3×10^5 [kg]
panel	mass: m_p	1.05×10^7 [kg]
	total size	1.5×1.4 [km]
	height	0.1 [m]
	thickness of top and bottom panels	0.5 [mm]
	size of sub-panel	100×100 [m]
	number of sub-panels	210 (15×14)
	Young's modulus	70 [GPa]
	Poisson's ratio	0.3
	coefficient of thermal expansion	2.3×10^{-5}[K^{-1}]
tethers	diameter	2.8 [mm]
	number of tethers	240 (16×15)
	vertical natural length: l_v	5.8 [km]
	Young's modulus	70 [GPa]

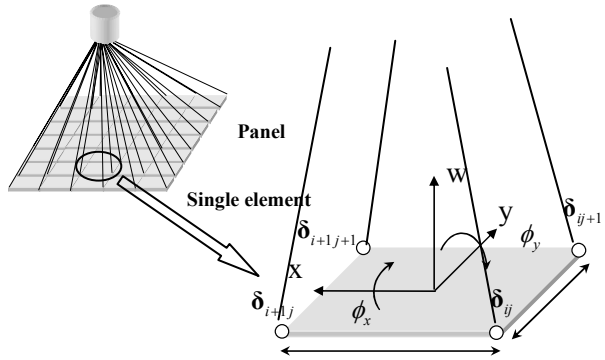

Fig. 2. Finite element

2.2. Equation of motion

As generalized coordinates, 3-2-1 Euler angles $\theta_x, \theta_y, \theta_z$ and displacement vector at all nodes $\boldsymbol{\delta}$ are used. Because the satellite is earth oriented, the satellite attitude is described by Euler angles with respect to the orbital coordinate. The x, y and z axes of the body coordinate system fixed at the mass center of the whole satellite correspond to the roll, pitch and yaw axes, respectively (Fig. 1). In the body coordinate system, the z axis is parallel to the line passing through the mass centers of the panel and the bus. The x and y axes are parallel to the projected edges of the panel on x-y plane. The displacement vector at all nodes $\boldsymbol{\delta}$ is defined as follows:

$$\boldsymbol{\delta} = \begin{bmatrix} w_{11} & \phi_{x11} & \phi_{y11} & w_{12} & \phi_{x12} & \cdots & \phi_{y1615} \end{bmatrix}^T \quad (1)$$

where $\phi_{x\,ij} = -\dfrac{\partial w_{ij}}{\partial y}$, $\phi_{y\,ij} = \dfrac{\partial w_{ij}}{\partial x}$, and w_{ij} is the displacement along -z axis at node *(i,j)* of the sub-panel (Fig. 2). The displacement w_{ij} is measured from the state in which the tether is of natural length with no load. The positive direction of w_{ij} is the -z direction.

Using the generalized coordinates, the energies can be derived as follows:

Kinetic Energy: T_m

$$T_m = T_{m\_trns} + T_{m\_rot} + T_{m\_vib}$$

$$T_{m\_trns} = \frac{1}{2} M \left\{ R\dot{\theta}^2 + m_r(1-m_r)(\dot{\boldsymbol{\delta}}^{\mathbf{T}}\mathbf{C_1}^{\mathbf{T}}\mathbf{C_1}\dot{\boldsymbol{\delta}} + (l_v + \mathbf{C_1}\boldsymbol{\delta})^2(\omega_x{}^2 + \omega_y{}^2)) \right\}$$

$$T_{m\_rot} = \frac{1}{2}\left(I_x\omega_x{}^2 + I_y\omega_y{}^2 + I_z\omega_z{}^2 \right)$$

$$T_{m\_vib} = \rho(\omega_x\omega_z\mathbf{C}_{rxx}\boldsymbol{\delta} + \omega_y\omega_z\mathbf{C}_{ryy}\boldsymbol{\delta} + \omega_y\mathbf{C}_{rxx}\dot{\boldsymbol{\delta}} - \omega_x\mathbf{C}_{ryy}\dot{\boldsymbol{\delta}})$$
$$+ \frac{1}{2}\left\{ \boldsymbol{\delta}^T(\mathbf{M_p} - m_p\mathbf{C_1}^{\mathbf{T}}\mathbf{C_1})\boldsymbol{\delta}(\omega_x{}^2 + \omega_y{}^2) + \dot{\boldsymbol{\delta}}^T(\mathbf{M_p} - m_p\mathbf{C_1}^{\mathbf{T}}\mathbf{C_1})\dot{\boldsymbol{\delta}} \right\}$$

where $\mathbf{C_1}\boldsymbol{\delta}$ corresponds to the displacement of the center of mass of the entire panel.

Gravitational Potential Energy: U_g

$$U_g = U_{g\_m} + U_{g\_res}$$

$$U_{g\_m} = -\frac{\mu M}{R}\left\{ 1 - \frac{1}{2} m_r(1-m_r)(1-3C_{OB\_33}{}^2)(l_v{}^2 + 2l_v\mathbf{C_1}\boldsymbol{\delta} + \boldsymbol{\delta}^{\mathbf{T}}\mathbf{C_1}^{\mathbf{T}}\mathbf{C_1}\boldsymbol{\delta}) \right\}$$

$$U_{g\_res} = -\frac{\mu}{R}\left\{ -\frac{1}{2R^2}\left((1-3C_{OB\_32}{}^2)(I_z - I_y) + (1-3C_{OB\_31}{}^2)(I_z - I_x) \right.\right.$$
$$+ (1-3C_{OB\_33}{}^2)\boldsymbol{\delta}^{\mathbf{T}}(\mathbf{M_p} - m_p\mathbf{C_1}^{\mathbf{T}}\mathbf{C_1})\boldsymbol{\delta}$$
$$\left.\left. + 6\rho(C_{OB\_31}C_{OB\_33}\mathbf{C_{rxx}} + C_{OB\_32}C_{OB\_33}\mathbf{C_{ryy}}) \right) \right\}$$

Strain Energy of the Panel : U_p

$$U_p = \sum_e U_{p\_e}$$

$$U_{p\_e} = \frac{1}{2}\boldsymbol{\delta}_e{}^T\mathbf{K_e}\boldsymbol{\delta}_e - k_T\delta_T\mathbf{C}_T\boldsymbol{\delta}_e$$

where the subscript e denotes the variables of each finite element. In the derivation, thermal stress is considered under the assumption of uniform temperature difference between the top and bottom sides of the panel.

Strain Energy of the tethers : U_t

$$U_t = \frac{1}{2}E_tA_t\boldsymbol{\delta}^T diag\left(\left[\frac{1}{l_{11}}\left(\frac{l_v}{l_{11}}\right)^2, 0, 0, \frac{1}{l_{12}}\left(\frac{l_v}{l_{12}}\right)^2, 0, \cdots, 0 \right] \right)\boldsymbol{\delta}$$

Using kinetic energy, potential energy and strain energy, Lagrange's equation of motion is derived. Under the assumption that $\theta_x, \theta_y, \theta_z$ and w_{ij}/l_v are so small that the higher orders of these terms can be neglected, the following equation of motion is obtained:

$$\mathbf{M}\ddot{\mathbf{x}} + \left(\mathbf{C}_m + \mathbf{C}_p + \mathbf{C}_t\right)\dot{\mathbf{x}} + \left(\mathbf{K}_m + \mathbf{K}_p + \mathbf{K}_t + \mathbf{K}_g\right)\mathbf{x} = \mathbf{f}_m + \mathbf{f}_g + \mathbf{f}_T(\delta_T) \quad (2)$$

where $\mathbf{x}^T = [\boldsymbol{\delta}^T \quad \theta_x \quad \theta_y \quad \theta_z]$, and the subscripts *m*, *g*, *p*, *t* and *T* indicate the terms caused by kinetic energy, gravitational potential energy, strain energy of the panel, strain energy of the tethers and thermal stress, respectively. The damping ratio $\zeta_1 = 0.005$ in the first mode of structural vibration is used as structural damping. The damping matrix $\mathbf{C}_p + \mathbf{C}_t$ is defined as follows:

$$\mathbf{C}_p + \mathbf{C}_t = \beta(\mathbf{K}_p + \mathbf{K}_t), \quad \beta = 2\zeta_1/\omega_1$$

where ω_1 is the natural angular frequency of the first mode.

3. Fundamental Dynamic Characteristics

3.1. Natural Frequency at the Equilibrium Point

At first, the panel deformation at the equilibrium point of Eq. (2) without temperature difference between the top and bottom sides is shown in Fig. 3. The origin of the z axis and w_{ij} is determined in the state without tether elongation. Therefore, deformation along the +z axis at each node corresponds to tether elongation. Please note that the direction of w_{ij} is the opposite of the z axis. Here, the connecting rigidity between sub-panels is assumed to be as stiff as the panel itself, indicating one large flexible panel suspended by multi-tethers. In this case, tether elongation is within 50 [cm] at LEO, and 2.1 [mm] at GEO. In Fig. 3, all tethers are elongated, and so no tethers are slack. However, slack tethers may occur as a result of dynamic panel deformation because the tether elongation is not so large. Figure 4 shows the distribution of tether tension in the case of LEO. The bar length and direction indicate the tension of tethers normalized by maximum tension and the direction of the tension, respectively. In the case of LEO, the maximum tension is only 35 [N]. The tension of the tethers is in approximate proportion to the panel deformation along the -z axis at each node. A bar length of zero indicates a slack tether. However, Fig. 4 shows no slack tethers.

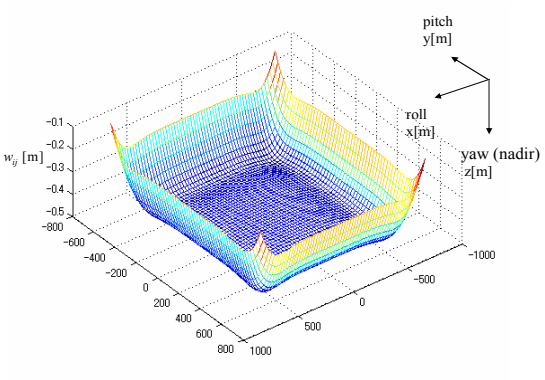

(a) Panel deformation at LEO (altitude 500 [km])

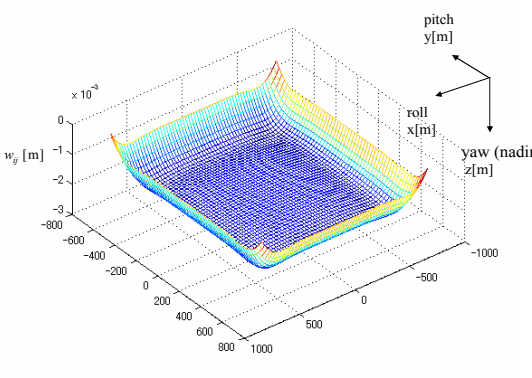

(b) Panel deformation at GEO

Fig. 3. Panel deformation without temperature difference

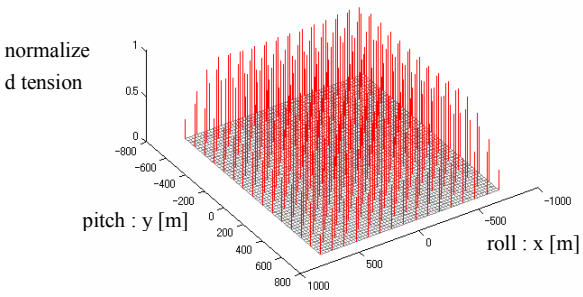

Fig. 4. Distribution of tether tension (LEO)

Next, the natural frequencies around the equilibrium point and the corresponding mode shapes at LEO and GEO are shown in Figs. 5 and 6, respectively. Here, the amplitude of panel deformation is assumed to be small enough not to cause slack tethers. In this case, coupling between panel bending and attitude motion is not observed because the natural frequency of panel bending is sufficiently higher than that of attitude motion if no tethers are slack. In the first mode of panel bending of Figs. 5 and 6, the center of the panel becomes a node. This is because the natural lengths of the tethers near the center of the panel are shorter than those at the outer edge of the panel, and the spring constant of the tethers is higher near the center. Thus, dynamic characteristics such as the natural frequency and the mode shapes of this structure are mainly determined by the spring constant of the tethers. Therefore, in the next section, we investigate the relationship between the tether stiffness and the coupling effect.

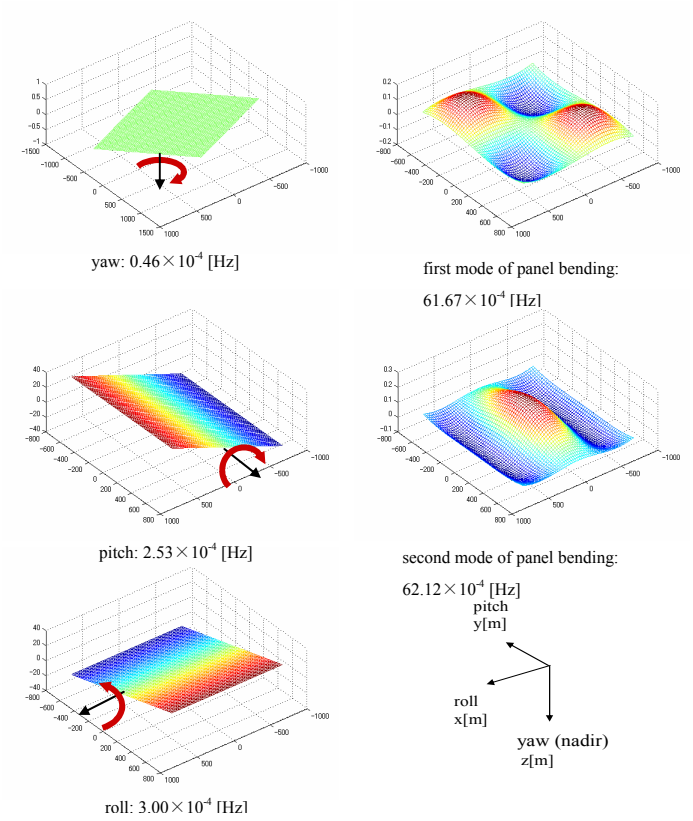

Fig. 5. Natural frequencies and mode shapes at LEO without tether slack (diameter of tethers: 2.8e-3 [m])

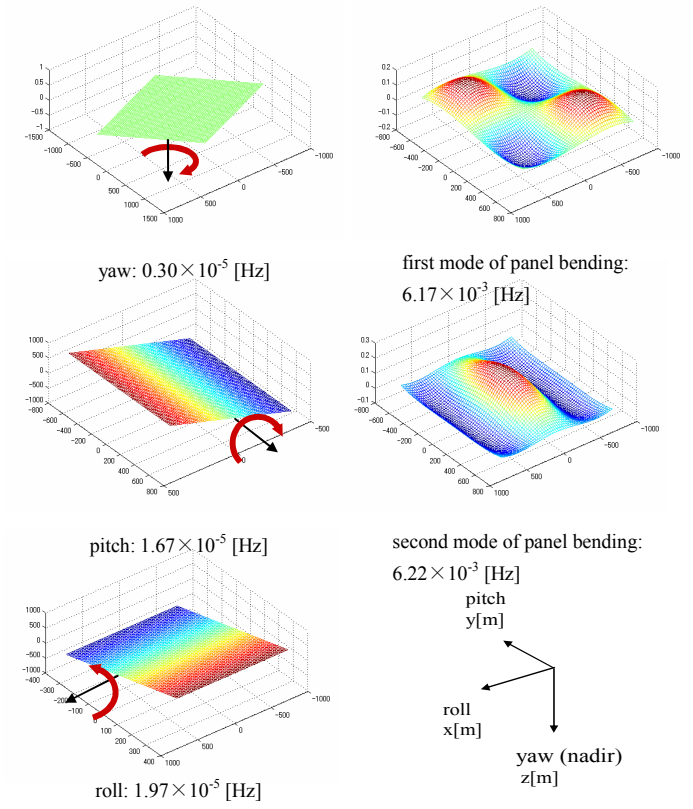

Fig. 6. Natural frequencies and mode shapes at GEO without tether slack (diameter of tethers: 2.8e-3 [m])

3.2. Effect of tether stiffness on the natural frequency

In order to investigate the effect of tether stiffness on natural frequency, the natural frequencies and the mode shapes are calculated for tethers of various diameters. The relationship between tether diameter and natural frequencies is shown in Fig. 7. The equilibrium states differ depending on the tether diameter. Because the natural frequencies of the first and second modes of panel bending are very similar, they appear to overlap in Fig. 7. From the figure, the natural frequencies of panel bending are shown to be of the same order as the natural frequency of attitude motion if the tether diameter is less than 3e-4 [m] at LEO. At GEO, however, the natural frequencies of panel bending are much higher than that of attitude motion if the tether diameter is within the range considered herein.

As examples, the natural frequencies and mode shapes for tethers of 2e-4 [m] in diameter at LEO and GEO are shown in Figs. 8 and 9, respectively. Figure 8 shows that panel bending is observed in the mode shapes of attitude motions and that attitude motions are observed in the panel bending. That is, coupling between structural deformation and attitude motion occurs in the case of tether diameters of 2e-4 [m] at LEO. In Fig. 9, however, no panel bending is observed in the mode shapes of attitude motions, although attitude motions are observed in the mode shapes of the panel bending. Therefore, it is shown that attitude motion without structural deformation can exists, even though low modes of panel bending without attitude motion can not exist in the case of tether diameters of 2e-4 [m] at GEO.

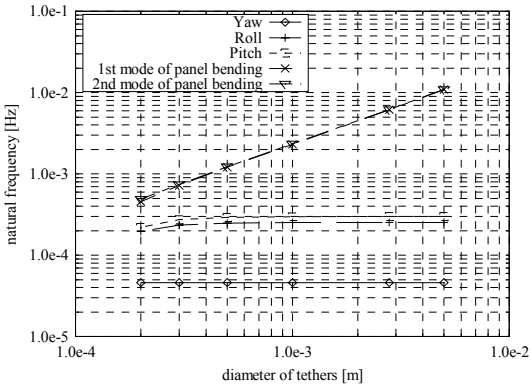

(a) LEO

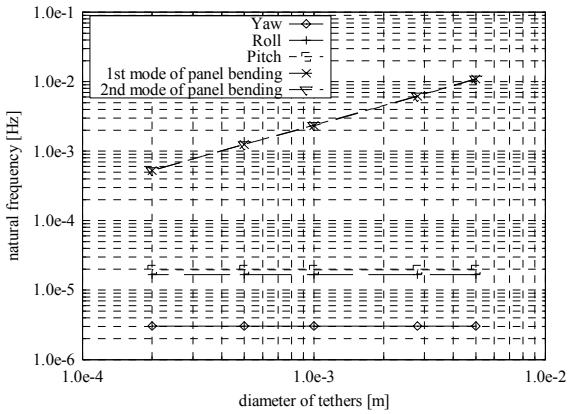

(b) GEO

Fig. 7. Relationship between diameter of tethers and natural frequencies

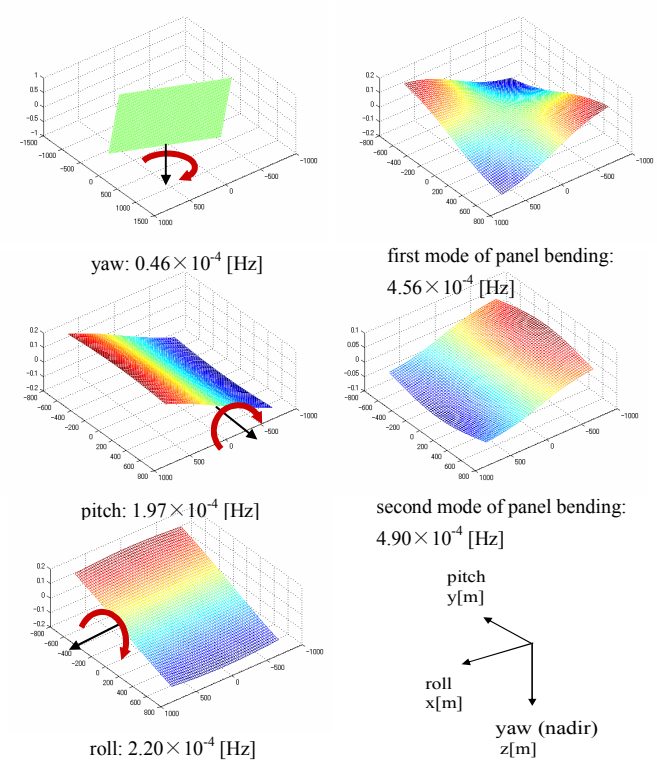

Fig. 8. Natural frequencies and mode shapes at LEO without tether slack (diameter of tethers: 2e-4 [m])

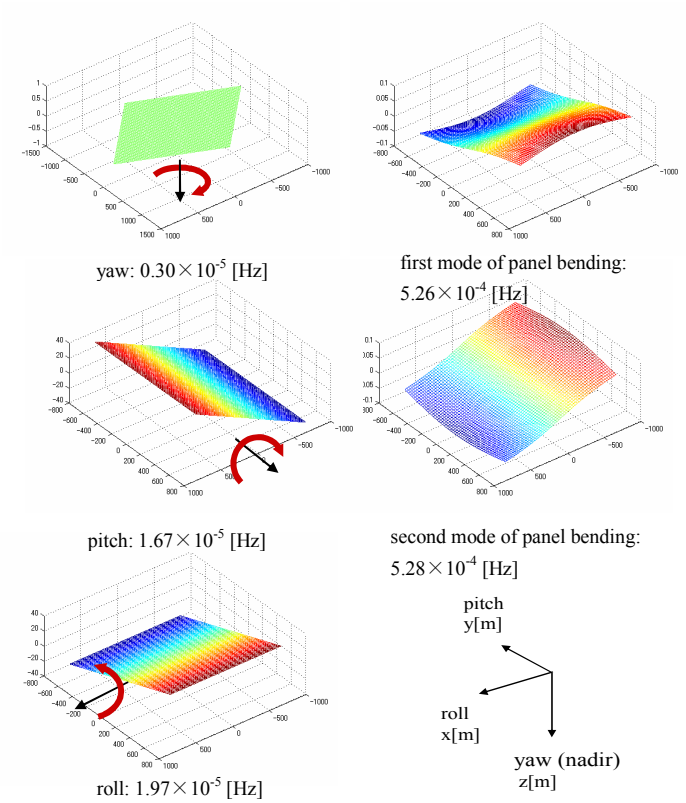

Fig. 9. Natural frequencies and mode shapes at GEO without tether slack (diameter of tethers: 2e-4 [m])

4. Effect of Tether Slack due to Thermal Deformation

4.1. Natural frequency with thermal deformation

In the previous section, it is shown that the coupling between structural deformation and attitude motion could occur for the small tether diameters. When the coupling occurs, periodic input to the structure, such as thermal input, could have an adverse influence on the attitude motion. Thermal deformation could also cause tether slack. The effect of tether slack on the natural frequency may be similar to the effect of the decrease of tether diameter. Therefore, thermal deformation induced by thermal input should be considered for further investigation.

In this section, panel deformation due to thermal stress and tether slack is investigated. A preliminary survey shows that the temperature difference between top and bottom sides of panel δ_T (temperature of the bottom side of the panel subtracted from that of the top side of the panel) would vary from approximately +25 to -30 [°C], depending on the angle of the panel with respect to the sun. If the connecting rigidity between sub-panels is as stiff as the panel itself, then a large deformation is caused by temperature difference δ_T. However, small temperature differences are tried in the following analysis in order to hold true the presuppositions of small strain and small deformation. If the tether slack and the coupling occurs due to the small temperature differences, larger scale or more complicated slack and the coupling would also be expected for the large temperature differences such as +25 and -30℃.

As an example, the panel deformation for $\delta_T = -5$ [°C] at LEO is shown in Fig. 10. When the temperature of the bottom side is higher than that of the top side, the edges of the panel are warped upward and most of displacements w_{ij} have positive values, except for some nodes near the center of the panel. The distribution of tether tension of this case is shown in Fig. 11, where the maximum tension is 177 [N]. The many tethers are slack at peripheral nodes. If most of the tethers are slack as in this case, the natural frequency of panel bending is expected to decrease greatly.

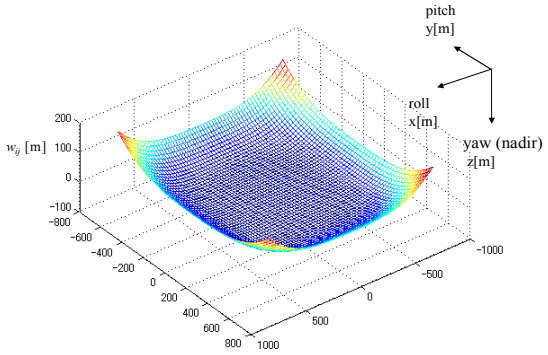

Fig. 10. Panel deformation ($\delta_T = -5$ [°C], LEO)

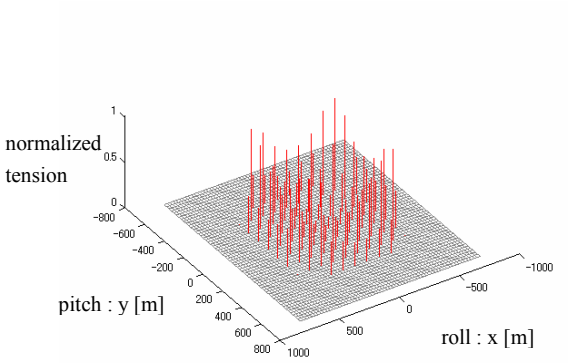

Fig. 11. Distribution of tether tension ($\delta_T = -5$ [°C], LEO)

The natural frequencies and corresponding mode shapes for $\delta_T = -5$ [°C] at LEO under the assumption that slack tethers have no rigidity are shown in Fig. 12. In this case, tethers at the edges of the panel are slack. Therefore, the bending rigidity of the panel decreases so much that coupling between panel bending and attitude motion, such as pitch and roll motions, is observed. Comparing Figs. 5 and 12 reveals that the order of magnitude of the natural frequencies of panel bending is reduced by one, becoming identical to those of attitude motion. Briefly, if the slack tethers were caused by thermal deformation, then the natural frequency of the structure could decrease, and coupling between panel bending and attitude motion could occur.

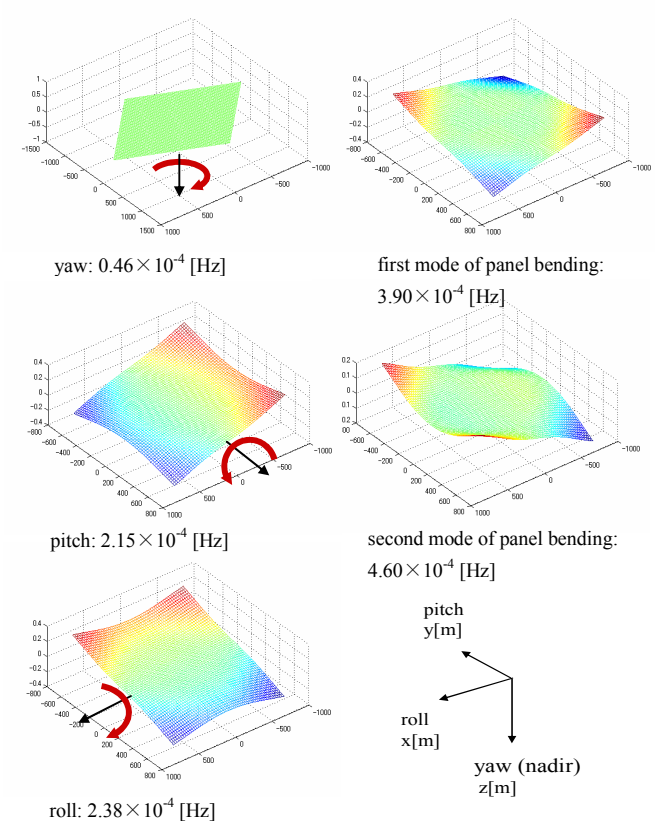

Fig. 12. Natural frequencies and mode shapes at LEO with tether slack ($\delta_T = -5$ [°C], diameter of tethers: 2.8e-3 [m])

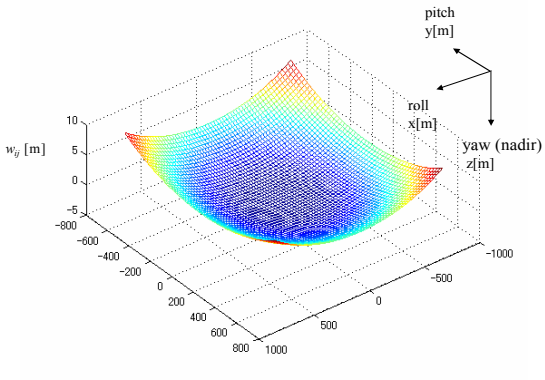

Fig.13. Panel deformation ($\delta_T = -0.1$ [°C], GEO)

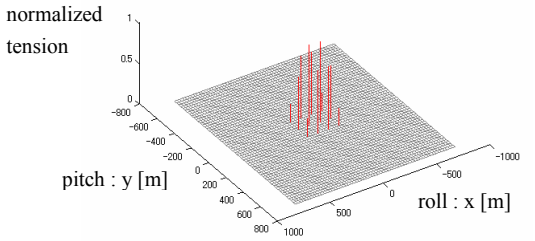

Fig. 14. Distribution of tether tension ($\delta_T = -0.1$ [°C], GEO)

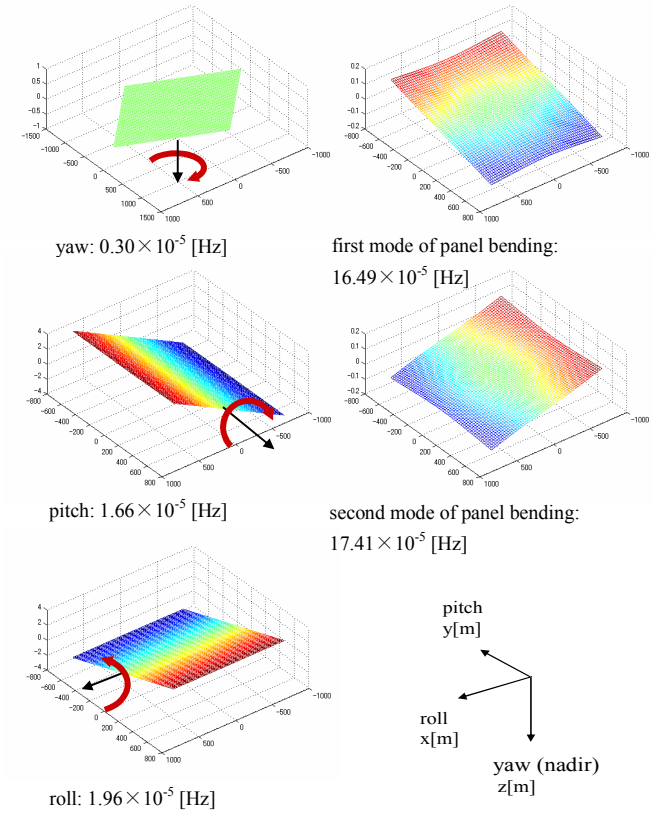

Fig. 15. Natural frequencies and mode shapes at GEO with tether slack ($\delta_T = -0.1$ [°C] , diameter of tethers: 2.8e-3[m])

Panel deformation and natural frequencies are calculated at GEO as well as LEO. As an example, the results for the temperature difference $\delta_T = -0.1$ [°C] at GEO are shown in Figs. 13-15. The edges of the panel are warped upward, and almost all of the tethers, except for those near the center, are slack (Figs. 13 and 14). In this case, the maximum tension is 40 [N]. Comparing Figs. 6 and 15 reveals that the order of magnitude of the natural frequencies of panel bending is reduced by one, becoming similar to those of attitude motion. Therefore, weak coupling between panel bending and attitude motion (roll/pitch) is observed in the mode shapes of panel bending (Fig. 15).

4.2. Dynamic simulations

In this section, dynamic simulations are carried out to investigate the attitude motion induced by periodic thermal input followed by orbital motion. Equation (2) is integrated numerically with the initial conditions shown in Table 2. As the periodic thermal input, the temperature difference between top and bottom sides of the panel is set in accordance with orbital motion (Fig. 16).

Table 2 Initial conditions

Euler angles: $\theta_x, \theta_y, \theta_z$	(0,0,0)
angular velocities: $\dot{\theta}_x, \dot{\theta}_y, \dot{\theta}_z$	$0.1 * \dot{\theta}$ (10% of orbital angular velocity)
displacement vector: $\boldsymbol{\delta}$	panel deformation at equilibrium point (Fig. 2)
rate of change of displacement vector: $\dot{\boldsymbol{\delta}}$	**0**

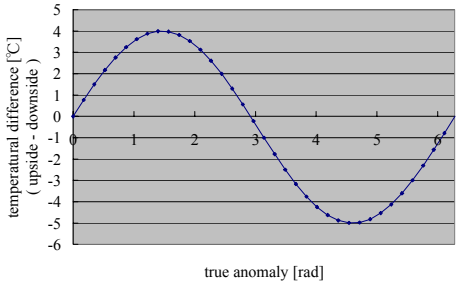

Fig. 16. Time history of temperature difference between top and bottom sides of the panel

In Fig.17, induced attitude motion with respect to the amplitude of the periodic thermal input is summarized. The amplitude of the periodic thermal input varies from 1/10 to equi-multiple of that shown in Fig. 16. The horizontal axis in Fig. 17 shows the normalized amplitude of the periodic thermal input. The induced attitude motion is evaluated by the maximum angle in 10 periods of orbit. Though applied amplitude is not so large compared with the value preliminary surveyed (from +25 to -30 [°C]), the induced attitude motion increases according to the increase of the thermal input. Furthermore, divergent tendencies are observed in the case of large thermal input. As a representative result, the time histories of panel deformation and Euler angles are obtained as shown in Figs. 18 and 19. In these results, the periodic thermal input in Fig. 16 is applied. The results correspond to the right end in Fig.17. Due to the periodic thermal input, the panel deforms and vibrates largely as shown in Fig.18. The large deformation of the panel causes slack in most of the tethers. Consequently, coupling between panel bending and attitude motion occurs. Comparing the Euler angles with and

without temperature difference (Fig. 19) reveals the following behavior:

(i) Due to the thermal input, attitude motion could be induced by panel bending.

(ii) The periodic thermal input could lead to divergent tendencies of the attitude motion, especially with respect to roll and yaw angles.

Therefore, some modification is required in order to reduce such thermal deformation.

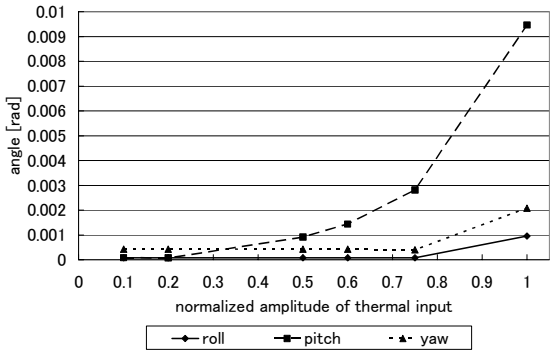

Fig. 17. Induced attitude motion with respect to the amplitude of the periodic thermal input

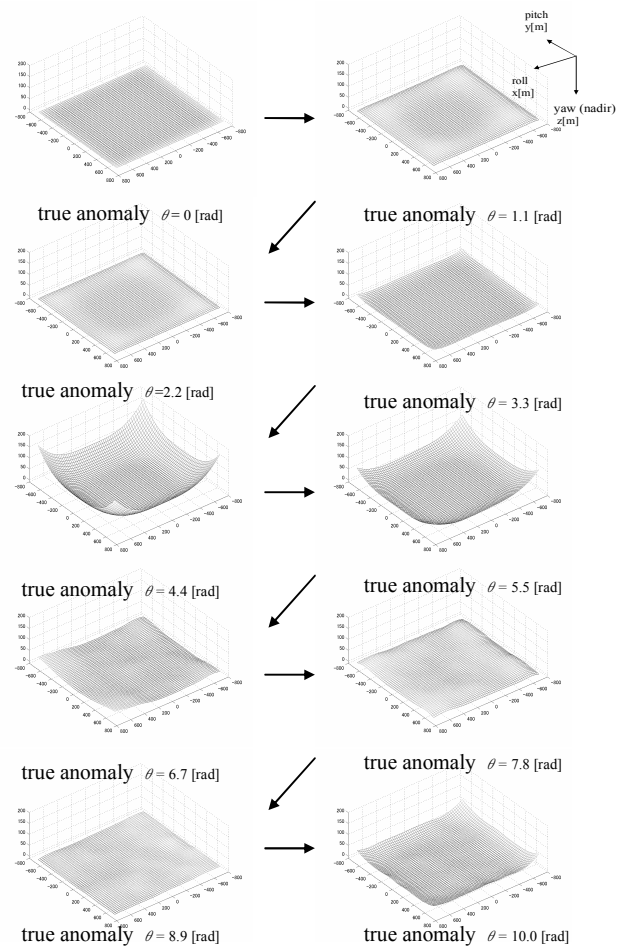

Fig. 18. Time histories of panel deformation with temperature difference

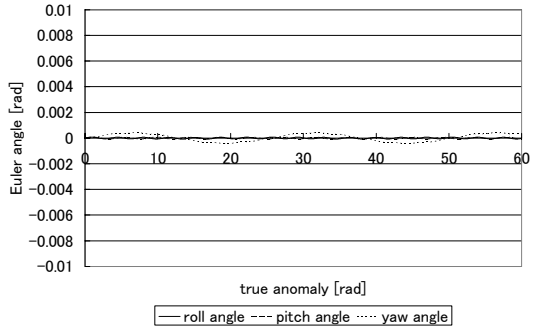

(a) simulation result without temperature difference of the panel

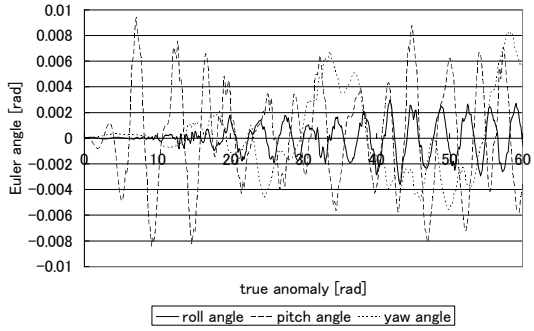

(b) simulation result with periodic temperature difference of the panel

Fig. 19. Time histories of Euler angles

5. Modification of the Structure

5.1. Modified model

In order to reduce the thermal deformation, localization of overall deformation is attempted. In order to relax the overall thermal deformation, the condition of the connection between sub-panels is modified. In the original model, the connecting rigidity between sub-panels is as stiff as the panel itself. Therefore, translational and rotational displacements are continuous between sub-panels at the edges. In the modified model shown in Fig. 20, the connection between sub-panels is changed to pin joints at the corners where rotation is free but translation is continuous.

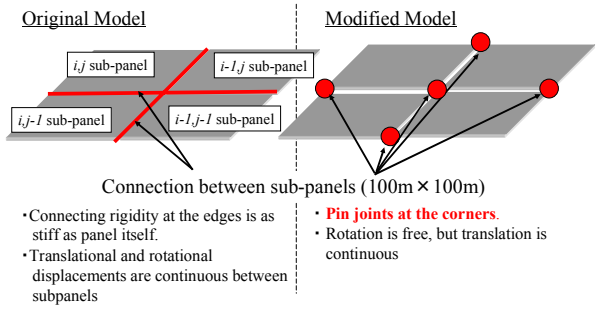

Fig. 20. Modification of the structure

The panel deformation of the modified model is shown in Fig. 21. Comparison of Figs. 10 and 21(b) reveals that the modified model can realize discretization of the overall thermal deformation. Furthermore, it is confirmed that there are no slack

tethers in the modified model. The natural frequencies and the mode shapes of the modified model are also confirmed to be very similar to those of Fig. 5 with no slack tethers. As such, the result is not shown here.

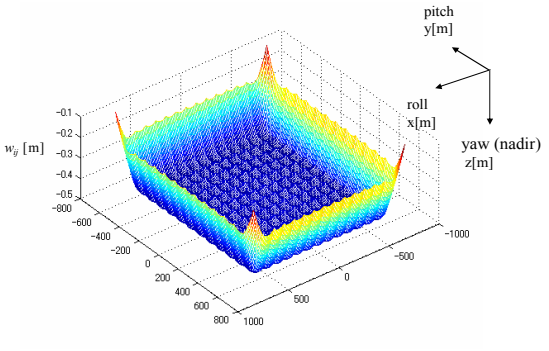

(a) temperature difference of panel: $\delta_T = 0$ [°C]

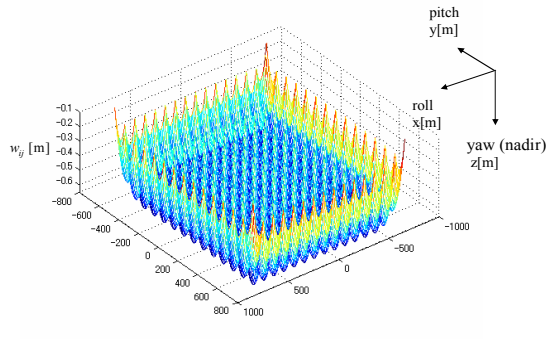

(b) temperature difference of panel: $\delta_T = -5$ [°C]

Fig. 21. Panel deformation of modified model at LEO

5.2. Dynamic simulation for the modified planar structure

In this section, we attempt to show that suppression of slack tethers in the modified model can avoid coupling between panel bending and attitude motion. If the coupling can be avoided, then the thermally induced attitude motion would become small. Dynamic simulations for the modified model are carried out in the manner described in section 4.2. The result is shown in Fig.22, where the parameters are the same as in Fig. 19(b). Comparison of Figs. 19(b) and 22 reveals that the thermally induced attitude motion is reduced to within ±0.002 [rad], which is extremely small.

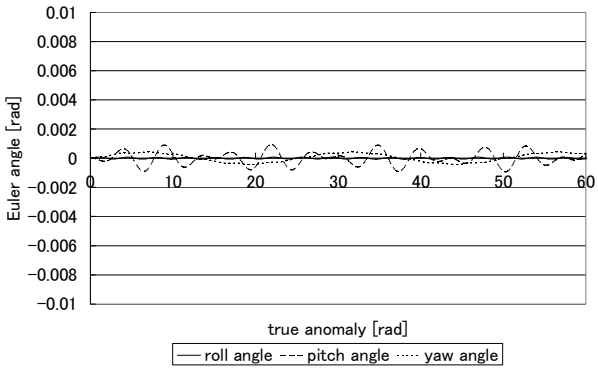

Fig. 22. Time history of Euler angles of the modified model with periodic temperature difference of the panel

6 Conclusions

Coupling between structural deformation and attitude motion of a large planar space structure suspended by multi-tethers was investigated. As a result, decreased tether stiffness is shown to be one of the dominant factors that lead to this coupling. The effect of tether slack on the natural frequency is similar to that of decreased tether stiffness. Tether slack was shown to be potentially induced by thermal deformation.

The simulation revealed the following:

(i) Most tethers could be slacked by periodic thermal input of small amplitude, and attitude motion could be induced by panel bending.

(ii) The periodic thermal input could lead to divergent tendencies of the attitude motion, especially with respect to roll and yaw angles.

Finally, the planar structure was modified to suppress the overall deformation of the structure. It was shown that the modified planar structure can release thermal deformation locally and suppress tether slack. The natural frequency of the modified structure did not decrease, and as a result, the thermally induced attitude motion becomes sufficiently small. Therefore, the modified planar structure suspended by multi-tethers is a potential candidate for large planar space structures.

Acknowledgement

The authors would like to thank Prof. S. Sasaki (ISAS/JAXA) for his useful discussion. This research was partly supported by the Grant-in-Aid for Young Scientists (B), 14750716, 2004, the ministry of education, culture, sports, science and technology.

References

[1] Modi V.J., Attitude Dynamics With Flexible Appendages – A Brief Review, Journal of Spacecraft and Rockets, 11 (1974) 743-751.

[2] R. B. Malla, Structural and orbital conditions on response of large space structures, Journal of Aerospace Engineering, 6(2) (1993) 115-132.

[3] K. Ishimura and K. Higuchi, The Effect of Axial Vibration of Large Structures on the Pitch Motion, the 24th International Symposium on Space Technology and Science (ISTS), 2004-c-15, 2004.

[4] B. Wie and C. Roithmayr, Integrated Orbit, Attitude, and Structural Control System Design for Space Solar Power Satellites, AIAA Guidance, Navigation, and Control Conference & Exhibit, Montreal, Canada, AIAA 2001-4273, 2001.

[5] J. D. Johnston and E. A. Thornton, Thermally Induced Dynamics of Satellite Solar Panels, Journal of Spacecraft and Rockets, 37(5) (2000) 604-613.

[6] Sang-Young Park, Thermally Induced Attitude Disturbance Control for Spacecraft with Flexible Boom, Engineering Note, Journal of Spacecraft and Rockets, 39(2), (2002), 325-328.

[7] B. Bigdeli, A Finite Element Thermal-Structural Analysis of the Mast of the International Space Station, 41st AIAA/ASME/ASCE/AHS/ASC Structures, Structural Dynamics, and Materials Conference and Exhibit, Atlanta, GA, April, 2000.

[8] S. Sasaki, K. Tanaka, K. Higuchi, N. Okuizumi, S. Kawasaki, M. Shinohara, K. Senda, K. Ishimura, and USEF SSPS Study Team, Tethered Solar Power Satellite, JAXA Research and Development Report, JAXA RR-03-005E, March 2004.

[9] T. Saito, Y. Kobayashi and H. Kanai, Concept Study of Space Solar Power Systems in USEF, 55th International Astronautical Congress, IAC-04-R.1.02, 2004.